ATLAS NOTE

ATLAS-COM-CONF-2014-004

February 25, 2014

Calibration of b-tagging using dileptonic top pair events in a combinatorial likelihood approach with the ATLAS experiment

The ATLAS Collaboration

Abstract

This note presents a new method to derive the b-jet tagging efficiency from data using a combinatorial likelihood approach applied to dileptonic $t\bar{t}$ events. Calibration results are obtained for the pp collision data collected by the ATLAS experiment at the Large Hadron Collider at $\sqrt{s} = 8$ TeV, corresponding to an integrated luminosity of $20.3\,\text{fb}^{-1}$. The b-jet tagging efficiency measurements are provided in the form of jet transverse momentum dependent scale factors which correct the b-tagging performance in simulation to that observed in data. The scale factors have been measured in the range 20–300 GeV and have a total uncertainty $\sim 2\,\%$ for jets with transverse momenta around 100 GeV. This represents a significant improvement in precision compared to alternative calibration methods.

ATLAS-CONF-2014-004
25 February 2014

1 Introduction

The ability to identify the flavour of a jet, separating b from c and uds/g (light-flavour) jets, is a crucial tool for much of the physics programme of the ATLAS [1] experiment at the Large Hadron Collider (LHC). Various b-tagging algorithms have been developed in ATLAS to achieve high b-tagging efficiencies for real b jets whilst keeping the misidentification efficiency for c and light-flavour jets at very low levels, based on optimisation studies performed using a full simulation [2] of the ATLAS detector. They range from relatively simple algorithms based on impact parameters (IP3D) and secondary vertices (SV1) to a more refined algorithm exploiting the topology of weak b- and c-hadron decays (JetFitter), all of which are documented in Ref. [3]. The most discriminating variables resulting from these algorithms are combined in artificial neural networks, and output weight probabilities are evaluated separately for b, c, and light-flavour jets. Finally, multivariate tagging algorithms based on these probabilities are used to further enhance the tagging performance. One of these is the MV1 algorithm used to illustrate the present calibration analysis. This is the most commonly used flavour tagging algorithm in ATLAS.

In order to take possible differences between the Monte Carlo (MC) simulation and real data into account, the b-tagging algorithms need to be calibrated in data. Several methods have been developed to measure the b-jet efficiency, the c-jet efficiency and the mistag rate in data [4–7]. This note describes a novel method using a combinatorial likelihood to measure the b-jet tagging efficiency in a data sample of $t\bar{t}$ events with two oppositely charged leptons in the final state, i.e., selecting top pair events where both W bosons from the top quark decays ($t \to W + b$)[1] in turn decay leptonically. Compared to previous calibrations [5] a large gain in precision is obtained by considering the correlations between the jets in the events, which results in reduced uncertainties when requiring b-tagged jets in analyses.

The calibration described in this note applies to cases where a fixed cut is applied to the discriminant distribution of the MV1 tagger, which is trained to yield high (low) values for b (light-flavour) jets. The results shown correspond to an overall 70% efficiency for b jets, as evaluated on a sample of simulated $t\bar{t}$ events and with jets with transverse momenta, p_{T}, and pseudorapidities, η [2], satisfying $p_{\mathrm{T}} > 20$ GeV and $|\eta| < 2.5$. The calibration results are presented in the form of data/simulation efficiency scale factors (SF), where $\mathrm{SF} \equiv \epsilon_b^{\mathrm{data}}/\epsilon_b^{\mathrm{sim}}$, and $\epsilon_b^{\mathrm{data}}$ ($\epsilon_b^{\mathrm{sim}}$) are the b-jet tagging efficiencies measured on data (simulation), respectively.

Descriptions of the Monte Carlo simulation samples, the object and event selection, the corrections applied to the simulated samples and the flavour composition are outlined in Section 2. Section 3 describes and motivates the likelihood method, followed by a discussion of the systematic uncertainties in Section 4. The note finishes with a presentation of the calibration results in Section 5 and conclusions in Section 6.

2 Data samples and event selection

The analysis described in this note uses an integrated luminosity of $20.3\,\mathrm{fb}^{-1}$ collected by the ATLAS experiment in 2012, at a centre-of-mass energy $\sqrt{s} = 8$ TeV. Events are required to satisfy standard data quality requirements, ensuring that all ATLAS detector components were functioning normally.

Events are required to pass a single-electron, single-muon or dilepton trigger. For the single lepton triggers, the OR of a lower threshold trigger (24 GeV) featuring an isolation requirement and a higher threshold trigger (e : 60 GeV μ : 36 GeV), without this requirement are used. The dilepton triggers have

[1] This analysis assumes the Standard Model top decay.

[2] ATLAS uses a right-handed coordinate system with its origin at the nominal interaction point in the centre of the detector, and the z axis along the beam line. The x axis points to the centre of the LHC ring, and the y axis points upwards. Cylindrical coordinates (r, ϕ) are used in the transverse plane, with ϕ being the azimuthal angle around the beam line. The pseudorapidity η is defined in terms of the polar angle θ as $\eta = -\ln\tan(\theta/2)$.

a threshold of 12 GeV for electrons and 13 GeV for muons. This combination of triggers is close to fully efficient for events passing the event selection criteria detailed in Sec. 2.2.

2.1 Simulated samples

This analysis requires several inputs to be taken from Monte Carlo simulation, including the expected flavour composition of the sample, and the p_{T} and η distributions of the selected jets. The ATLAS simulation infrastructure is described in more detail in Ref. [2].

The main $t\bar{t}$ production process has been generated using Powheg [8] interfaced to Pythia6 [9] with the Perugia 2011C tune [10] for the parton shower and hadronisation, and CT10 parton density functions (PDFs) [11]. An alternative $t\bar{t}$ sample has been produced with Alpgen [12] interfaced to Herwig [13] and Jimmy [14], with the CTEQ6L1 PDFs [15]. The Alpgen sample includes the explicit production of $t\bar{t}b\bar{b}$ and $t\bar{t}c\bar{c}$ in the matrix element. The effects of initial and final state radiation (ISR/FSR) uncertainties are studied using two fast simulation samples generated with AcerMC [16] and the CTEQ61 PDFs interfaced to Pythia6, with two tunes that span the variations compatible with ATLAS studies of additional jet activity in $t\bar{t}$ events [17]. Finally, fast simulation samples generated with Powheg using the CT10 PDFs interfaced to Herwig with the AUET2 [18] tune or Pythia6 with the AUET2B tune [19] are used for further studies of hadronisation uncertainties. Most of the simulated $t\bar{t}$ samples correspond to about five times the data statistics.

Backgrounds containing two real isolated leptons include single-top production in association with a W boson (Wt), Z+jets events with $Z \to \tau\tau$ and leptonic τ lepton decays, and diboson production (WW, WZ and ZZ) with leptonic boson decays.

Single-top production in the Wt and s-channel modes has been generated using Powheg interfaced to Pythia6 with the Perugia 2011C tune for the parton shower and hadronisation, and CT10 PDFs. The t-channel single-top processes have been simulated with the AcerMC generator again interfaced to Pythia6 with the Perugia2011C tune. For single-top Wt production, two additional samples have been produced with AcerMC + Pythia, again with the parton shower tuned to yield a higher or lower level of radiation.

The Alpgen generator is used for the diboson samples interfaced to Herwig and Jimmy with the AUET2 tune. For systematic studies the diboson processes have also been generated using Herwig, with CTEQ6L1 PDFs and the AUET2 tune for the parton shower and hadronisation model.

The $Z+ \geq 1b$, $Z+ \geq 1c$ and $Z+ \geq 1$ light-jet events have been simulated with the Sherpa generator [20], using CTEQ6L1 PDFs. The W+jets background, including $W+ \geq 1b$, $W+ \geq 1c$ and $W+ \geq 1$ light-jet events, has also been simulated with Sherpa using the same settings. For systematic studies, Z+jets production has also been simulated using Alpgen, interfaced with Pythia for the showering and the underlying event.

The impact of including the Standard Model Higgs boson production as a background was also tested, fixing the Higgs-boson mass to 125 GeV, and considering the $gg \to H(H \to WW)$, $ZH(Z \to \ell^+\ell^-$, $H \to b\bar{b})$ and $t\bar{t}H$ ($H \to b\bar{b}$ and $H \to WW$) channels. The contribution was found to be negligible.

Lepton fake events, where at least one lepton is non-prompt (i.e. from a b/c hadron decay, conversion or hadronic fake), are estimated from real data by changing the selection criteria from opposite sign leptons to same sign leptons [21]. The resulting sample is predicted to be very pure in fake e/μ events and directly applicable as a prediction in the opposite-sign signal sample. The contribution from same-sign leptons predicted by the simulation samples is subtracted from the same sign data sample to avoid double counting.

2.2 Object and event selection

The key objects for b-tagging are the calorimeter jets, the tracks reconstructed in the inner detector, and the selected primary vertex. The tracks are associated with the calorimeter jets based on their distances $\Delta R \equiv \sqrt{\Delta\eta^2 + \Delta\phi^2}$ [22]. The track selection criteria depend on the b-tagging algorithm, and are detailed in Refs. [3, 23].

Events are required to have at least one reconstructed primary vertex with at least five associated tracks. The vertex with the highest sum of squared transverse momenta of the associated tracks is selected as the primary vertex. Jets are reconstructed from topological clusters [1] formed from energy deposits in the calorimeter using the anti-k_t algorithm with a distance parameter of 0.4 [24–26]. They are then corrected to the hadronic scale with appropriate calibration factors. Two approaches towards jet clustering are employed by ATLAS: one starting from clusters at the electromagnetic scale ("EM jets"), and one starting from clusters calibrated using the local cluster weighting method ("LC jets"). The measured jet energies are corrected using the jet area method [27, 28] to reduce effects due to additional proton-proton interactions in the same or neighbouring bunch crossings, referred to as pile-up in the following. The results shown in this note pertain to EM jets; the procedure and results obtained for LC jets are very similar. Jets are calibrated using a p_{T}- and η-dependent simulation-based calibration scheme, with in-situ corrections based on data. Only jets with $p_{\mathrm{T}} > 20$ GeV and $|\eta| < 2.5$ are used for this analysis. The "jet vertex fraction" (the ratio of the sum of the p_{T} of tracks associated with the jet and also associated with the selected primary vertex to that of all tracks associated with the jet) is used to reduce the effects of pile-up. For jets with $p_{\mathrm{T}} < 50$ GeV and $|\eta| < 2.4$ it is required to exceed 0.5. The measurement of the jet energy, the jet energy scale determination and the specific cuts used to reject jets of bad quality are described in Ref. [29]. For a jet with $p_{\mathrm{T}} = 100$ GeV the uncertainty on the jet energy scale is $\sim 2\%$ [30].

Leptons are required to have transverse momentum above 25 GeV and pseudorapidity $|\eta| < 2.5$ ($|\eta| < 2.47$) for muons (electrons). In order to have a very pure lepton selection for both electrons and muons, a very tight identification requirement is made. Leptons are required to be isolated: the transverse momentum from charged particles with $p_{\mathrm{T}} > 400$ MeV in a cone of $\Delta R = 0.2$ around the lepton direction, excluding the lepton itself, is required to be less than 4 % of the lepton's transverse momentum; the energy collected in the calorimeter in a cone of $\Delta R = 0.3$ around the lepton direction and projected onto the transverse plane, after removing the lepton energy and subtracting the contribution expected from pile-up, is required to be less than 7 % of the lepton's transverse momentum. In addition, electrons are required to have a transverse impact parameter $|d_0| < 0.1$ mm with respect to the primary vertex while muons are required to have transverse and longitudinal impact parameters satisfying $|d_0| < 1$ mm and $|z_0 - z_{\mathrm{PV}}| < 10$ mm respectively. Looser selection criteria are used to identify leptons which fail the tight cuts, with the following cuts relaxed: the lepton transverse momentum must be $p_{\mathrm{T}} > 10$ GeV, no calorimeter isolation is required and the charged particle isolation requirement is required to be less than 10 %. Events are required to have exactly two oppositely charged leptons passing the tight selection criteria. The two leptons can be either either different or same flavour ($e\mu$ or $e^+e^-/\mu^+\mu^-$), with the same-flavour leptons combined into one channel. Events with any additional leptons that pass the looser selection requirement are vetoed.

Events with electrons with energy deposits in the transition region between the barrel and forward electromagnetic calorimeter ($1.37 < |\eta_{\mathrm{cal}}| < 1.52$) are also removed from the analysis. For single lepton triggered events one of the leptons is required to have satisfied the trigger requirement (or both for dilepton triggered events).

In the e^+e^- and $\mu^+\mu^-$ channels a significant contamination is expected from Drell-Yan $Z/\gamma^* \to \ell^+\ell^-$ production; this is suppressed by requiring that the dilepton invariant mass $m(\ell\ell)$ is not between 80 GeV and 100 GeV, and by requiring that the missing transverse energy exceeds $E_{\mathrm{T}}^{\mathrm{miss}} > 60$ GeV, where

$E_{\mathrm{T}}^{\mathrm{miss}} = \sqrt{\left(E_x^{\mathrm{miss}}\right)^2 + \left(E_y^{\mathrm{miss}}\right)^2}$. The $E_{\mathrm{T}}^{\mathrm{miss}}$ quantities used in this analysis are computed using calibrated calorimeter cells belonging to reconstructed high-p_{T} objects: electrons, photons, jets and muons, along with the calorimeter energy deposits not clustered in jets with $p_{\mathrm{T}} > 20$ GeV (soft-terms). In addition, the low mass region with $m(\ell^+\ell^-) < 50$ GeV is excluded for the same-flavour channel. After such cuts Z+jet production with $Z \to e^+e^-$ and $Z \to \mu^+\mu^-$ is still the dominant background, with $Z \to \tau^+\tau^-$ playing a smaller role.

When applying the selection to simulated events, the simulated distribution of the number of pile-up interactions is reweighted in order to reflect that measured in data. In addition, corrections are applied to electrons, muons and jets, in order to reflect the calibrations of the energy scale, energy resolution and object reconstruction and identification efficiencies as derived from data.

2.3 Corrections applied to simulated samples

Due to theoretical uncertainties on the cross sections and possible acceptance effects, Monte Carlo simulations are not expected to reproduce perfectly the normalisation of the different processes as observed in data. Therefore the normalisation of the Z+jets background, of the fake lepton contribution and of the top pair production signal are derived directly from data.

Monte Carlo to data normalisation factors for the the Z+jets background and the $t\bar{t}$ signal are derived with a maximum likelihood fit to the observed numbers of events in the signal regions and in dedicated Z+jets control regions defined separately for the four different channels, $e\mu$ and $e^+e^-/\mu^+\mu^-$, in both the two- and three-jet cases. The Z+jets control regions differ from their respective signal regions by a dilepton invariant mass requirement 80 GeV $< m(\ell\ell) <$ 100 GeV; for the $e\mu$ channels the corresponding region in the e^+e^- and $\mu^+\mu^-$ final states is used. For the same-flavour channel, the same cut on the missing transverse energy as for the signal region of $E_{\mathrm{T}}^{\mathrm{miss}} > 60$ GeV was applied. When varying systematic uncertainties the likelihood fit is rerun. The other backgrounds, including single top and diboson production, are fixed to their Monte Carlo expectation values. The normalisation factors are found to range from 0.99 to 1.11 for Z+jets and 1.07 to 1.11 for $t\bar{t}$.

The jet p_{T} spectrum in data is found to be softer than the prediction from the Powheg+Pythia $t\bar{t}$ sample. The distribution of the average p_{T} of the top and anti-top quark was reweighted at truth level according to the unfolded measurement performed on 2011 $\sqrt{s} = 7$ TeV data [31]. The full correction is conservatively taken to estimate the systematic uncertainty.

A good agreement of simulation with data is crucial for this analysis. The overall agreement of the Monte Carlo simulation with data has been checked in several kinematic distributions for all signal and control regions. After the application of the above-mentioned corrections, good agreement with simulation is seen in all distributions within the statistical precision of the data. As an example inclusive distributions for the $e\mu$ two-jet channel are shown in Fig. 1.

2.4 Flavour composition

The analysis is carried out separately in the $e\mu$ and $e^+e^-/\mu^+\mu^-$ channels for both the two and three-jet bins. The number of events expected from Monte Carlo simulation (after all corrections outlined in Section 2 have been applied) and in data for these four regions are presented below together with the expected flavour composition.

Table 1 shows the expectation from Monte Carlo simulation and data for the $e\mu$ channel. For the two-jet selection, the possible flavour combinations are bb, bj and jj, where b represents a b-jet and j is defined as a non b-jet[3]. For the three-jet selection, there are four possible combinations: bbb, bbj, bjj and jjj. The flavour contributions are identified by looking at the truth label of the jets using the standard

[3]The convention that j indicates any non b-jet is adopted here and throughout this note.

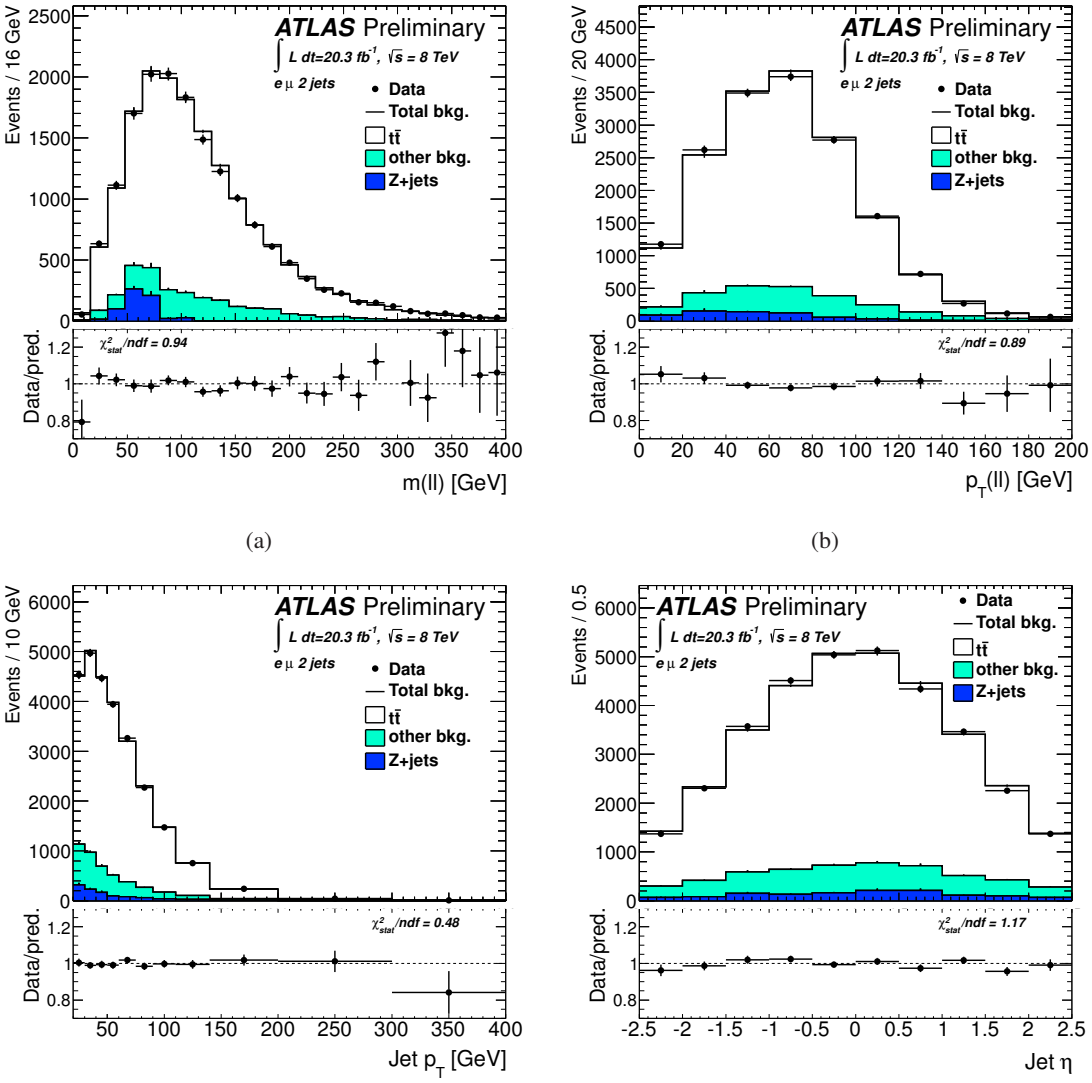

Figure 1: Control plots for the $e\mu$ 2 jet selection. The (a) $m(\ell^+\ell^-)$ (b) $p_{\mathrm{T}}(\ell^+\ell^-)$ (c) jet p_{T} and (d) jet η distributions are shown. The other bkg. component contains the contributions from single top, dibosons and lepton fakes. All corrections and Monte Carlo to data normalisation factors are applied to the simulated samples. The uncertainties are statistical only and the χ^2/ndf compares the data and total background shapes within these uncertainties.

ATLAS flavour labelling, based on the presence of a b-quark (or c-quark) after FSR within a radius of $\Delta R = 0.3$ from the jet axis. The top pair signal mainly contributes with bb and bj flavour combinations, with only a very small contribution from jj. The bj combinations reflect one b-jet from one of the top decays and a light-flavour jet either from initial or final state radiation. After adding the backgrounds, mainly irreducible single-top production (dominated by the Wt process), Z+jets production (dominated by $Z \to \tau^+\tau^-$ events) and diboson production (dominated by WW events), the jj contribution increases to 11 %. In order to correctly subtract the non-b-jet background for the measurement of the b-jet efficiency, the analysis therefore relies on two main ingredients: the correct estimation of the fraction of bj with respect to bb in top pair events, driven mainly by the theory modelling of top pair events, and a precise estimation of the non-top background. Due to the data driven procedure used to estimate the fake lepton contribution, the flavour composition of these events is not known. As such they are combined with the jj or jjj backgrounds with their b-tagging weight distributions estimated from data.

Even if the analysis explores per-event flavour correlations among the jets, it is still useful to quote the overal expected b-jet purity in the selected sample of events: in the two-jet case it is $\sim$ 75 %, while in the three-jet case it is $\sim$ 55 %.

Sample	$t\bar{t}$	Single top	Z+jets	Diboson	Total MC	Fakes	Data
2 jets	14106±36	1127±16	655±50	806±18	16693±66	209±14	16674
jj	307±5	64±4	516±50	790±17	1775±53		
bj	4091±19	714±13	30±2	15±2	4850±24		
bb	9708±30	349±9	10±1	1±0	10068±32		
jj [%]	2	6	94	98	11		
bj [%]	29	63	5	2	29		
bb [%]	69	31	2	0	60		
3 jets	10128±31	509±11	241±16	322±11	11200±38	124±11	11250
jjj	155±3	20±2	217±16	312±11	704±20		
bjj	2334±14	244±7	18±1	9±2	2605±16		
bbj	7512±26	242±7	6±1	1±1	7760±27		
bbb	127±3	2±1	0±0	0±0	129±3		
jjj [%]	2	4	90	97	6		
bjj [%]	23	48	8	3	23		
bbj [%]	74	48	2	0	69		
bbb [%]	1	0	0	0	1		

Table 1: The $e\mu$ channel. Numbers of selected events in data and simulation, and flavour composition in the simulation. The uncertainties are statistical only.

Table 2 shows the corresponding numbers for the $e^+e^-/\mu^+\mu^-$ channel. Single-top production and Z+jets production, with $Z \to e^+e^-$ and $Z \to \mu^+\mu^-$, are still the dominant backgrounds, with $Z \to \tau^+\tau^-$ playing a smaller role. The overall b-jet purity is $\sim$ 67 % in the two-jet case and $\sim$ 52 % in the three-jet case.

3 Efficiency determination

This section describes the method used for extracting the b-tagging efficiency. In Section 3.1 a simpler but similar analysis is described (the so-called kinematic selection analysis [5]). The techniques of this analysis motivate the more sophisticated technique that is used in this note, discussed in Section 3.2.

Sample	$t\bar{t}$	Single top	Z+jets	Diboson	Total MC	Fakes	Data
2 jets	5305±21	393±9	919±49	302±11	6919±55	58±8	6921
jj	129±3	18±2	839±49	295±11	1282±50		
bj	1649±12	253±7	62±2	6±2	1970±14		
bb	3528±18	121±5	17±1	0±0	3666±19		
jj [%]	2	5	91	98	19		
bj [%]	31	64	7	2	28		
bb [%]	66	31	2	0	53		
3 jets	3995±19	217±7	338±20	133±7	4683±29	34±6	4667
jjj	73±2	10±2	290±20	127±7	499±21		
bjj	979±10	97±5	33±2	5±2	1114±11		
bbj	2895±17	108±5	15±1	1±1	3019±17		
bbb	48±2	2±1	0±0	0±0	50±2		
jjj [%]	2	5	86	96	11		
bjj [%]	25	45	10	4	24		
bbj [%]	72	50	4	0	64		
bbb [%]	1	1	0	0	1		

Table 2: The $e^+e^-/\mu^+\mu^-$ channel. Number of selected events in data and simulation, and flavour composition in the simulation. The uncertainties are statistical only.

3.1 Equation-based methods to determine the *b*-tagging efficiency

In the kinematic selection analysis events are selected to obtain the highest possible b-jet purity. The selected jets are then treated as individual objects with any event level correlations between the jets neglected. In order to extract the efficiency, ϵ_b, corresponding to a certain b-tagging requirement the following equation is used:

$$f_{\text{tagged}} = f_b\epsilon_b + (1 - f_b)\epsilon_j, \tag{1}$$

where f_{tagged} is the fraction of jets selected by the b-tagging requirement, f_b is the fraction of b jets in the selected sample and ϵ_b (ϵ_j) is the b (non-b) jet efficiency. Using this equation ϵ_b can be calculated by measuring f_{tagged} from data with f_b and ϵ_j determined from MC simulation. This method has the advantage that it is relatively straightforward to measure the b-jet efficiency in bins of various 'jet related' kinematic quantities (e.g. p_{T}, η), since the jets can be simply binned as a function of such quantities before calculating ϵ_b. This method does not however take advantage of the event level correlation between the jet flavours which can be exploited to achieve greater precision.

For the case with exactly two jets in the event, one way to include this information is to generalise the single equation above to a system of two equations:

$$f_{2\text{ tags}} = f_{bb}\epsilon_b^2 + f_{bj}\epsilon_j\epsilon_b + \left(1 - f_{bb} - f_{bj}\right)\epsilon_j^2 \tag{2}$$

$$f_{1\text{ tag}} = 2f_{bb}\epsilon_b(1 - \epsilon_b) + f_{bj}\left[\epsilon_j(1 - \epsilon_b) + \left(1 - \epsilon_j\right)\epsilon_b\right] + \left(1 - f_{bb} - f_{bj}\right)2\epsilon_j\left(1 - \epsilon_j\right), \tag{3}$$

where $f_{1\text{ tags}}$ ($f_{2\text{ tags}}$) is the fraction of events with 1 (2) tagged jets and f_{bb} (f_{bj}) is the fraction of events with a true bb (bj) jet pair. The single jet flavour fraction in Eq. 1 is related to the new terms by $f_b = f_{bb} + f_{bj}/2$. The third flavour combination is $f_{jj} = 1 - f_{bb} - f_{bj}$ and is therefore redundant.

The two-equation formalism exploits additional information by applying a b-tag or anti b-tag requirement to the first jet with the b-jet purity of the second jet in the event increasing or decreasing accordingly. The additional information contained in the two equations can be exploited in two ways. Firstly, the b-tagging efficiency can be obtained by measuring both $f_{1\text{ tags}}$ and $f_{2\text{ tags}}$ from data, with f_{bb},

f_{bj} and ϵ_j taken from simulation. As additional information is included compared to the per-jet case, a higher precision on ϵ_b is expected. Secondly, as this is a set of two equations with only one unknown, the system is overconstrained. Therefore as an alternative an additional parameter could be determined from the data, for example f_{bb}/f_{bj}, which is sensitive to top modelling systematics taking the remaining unkowns, f_{jj} and ϵ_j from simulation. In this case a lower statistical precision on the measured value of ϵ_b is expected compared to the case with one unknown parameter.

When using two such equations the generalisation to a measurement of the b-jet tagging efficiency in bins of kinematic jet variables is however less straightforward. Here, the assumption is made that the b-tagging efficiencies of the two jets in the event are uncorrelated. If the analysis is done in N kinematic bins, each jet will populate one bin, resulting in N^2 combinations for two jets. For each of these combinations a system of two equations is needed, so in total there will be $2 \times N^2$ equations, with $2 \times N^2$ flavour fractions (the flavour fractions corresponding to the first jet being in one bin, the second in another one), N efficiencies for b jets and non-b jets. The system of equations is coupled by the efficiencies appearing as binomial terms and each of them being a function of the single jet kinematic bin, rather than of their combinations.

Although it is possible to solve such a system of non-linear equations, it is much simpler to model the same system using a more flexible and powerful likelihood function, using a numerical minimisation program (in this case MINUIT [32]) to solve the system by maximising a likelihood function. The likelihood formalism for both the two- and three-jet cases is described in the next subsection.

3.2 Likelihood fit-based approach to efficiency determination

The likelihood function considered in this analysis is an unbinned one. In the two jet case the following per-event likelihood function is adopted:

$$\begin{aligned} \mathcal{L}\left(p_{\mathrm{T},1}, p_{\mathrm{T},2}, w_1, w_2\right) = \quad & [\quad f_{bb}\mathcal{P}_{bb}\left(p_{\mathrm{T},1}, p_{\mathrm{T},2}\right)\mathcal{P}_b\left(w_1|p_{\mathrm{T},1}\right)\mathcal{P}_b\left(w_2|p_{\mathrm{T},2}\right) \\ & + \quad f_{bj}\mathcal{P}_{bj}\left(p_{\mathrm{T},1}, p_{\mathrm{T},2}\right)\mathcal{P}_b\left(w_1|p_{\mathrm{T},1}\right)\mathcal{P}_j\left(w_2|p_{\mathrm{T},2}\right) \\ & + \quad f_{jj}\mathcal{P}_{jj}\left(p_{\mathrm{T},1}, p_{\mathrm{T},2}\right)\mathcal{P}_j\left(w_1|p_{\mathrm{T},1}\right)\mathcal{P}_j\left(w_2|p_{\mathrm{T},2}\right) \\ & + \quad 1 \leftrightarrow 2 \;]/2, \end{aligned} \tag{4}$$

where:

- f_{bb}, f_{bj} and $f_{jj} = 1 - f_{bb} - f_{bj}$ are the overall two jet flavour fractions.
- $\mathcal{P}_f\left(w|p_{\mathrm{T}}\right)$ is the PDF (probability density function) for the b-tagging discriminant or *weight* for a jet of flavour f, for a given transverse momentum[4].
- $\mathcal{P}_{f_1 f_2}\left(p_{\mathrm{T},1}, p_{\mathrm{T},2}\right)$ is the two-dimensional PDF for $[p_{\mathrm{T},1}, p_{\mathrm{T},2}]$ for the flavour combination $[f_1, f_2]$.

In this analysis all the PDFs are implemented as binned histograms. For example, for N p_{T} bins, $\mathcal{P}_{f_1 f_2}\left(p_{\mathrm{T},1}, p_{\mathrm{T},2}\right)$ is expressed as an $N \times N$ binned histogram. For the symmetric bb and ll combinations, the PDF is symmetrised, reducing the number of independent bins to determine from $N^2 - 1$ to $N \times (N+1)/2 - 1$ which reduces the statistical fluctuations from Monte Carlo; as a consequence, the explicit symmetrisation expressed by Eqn. 4 for these combinations is for notational convenience only. The flavour PDFs $\mathcal{P}_f\left(w|p_{\mathrm{T}}\right)$ are defined in a similar way, with one binned histogram for each p_{T} bin. All PDFs are determined from simulation, except for the b-jet weight PDF, which contains the information to be extracted from the data.

For the case where only the b-tagging efficiencies for a single cut on the b-tagging discriminant distribution need to be extracted, a histogram with only two bins is needed to describe the b-weight PDF

[4]This means that, regardless of the p_{T} bin the jet falls in, the integral of the PDF over the b-tagging weight variable is one.

for each p_{T} bin, with the bin above the cut value corresponding to the b-tagging efficiency. The b-tagging efficiency corresponds then to

$$\epsilon_b\left(p_{\mathrm{T}}\right) = \int_{w_{\mathrm{cut}}}^{\infty} dw' \mathcal{P}_b\left(w', p_{\mathrm{T}}\right).$$

An extension of the method to extract the full b-jet b-weight PDF with an arbitrary binning in any jet kinematic quantity is straightforward, even if beyond the scope of this note.

The likelihood function distinguishes between the different flavour fractions, but not between signal and background processes. To extract the PDF corresponding to the b-jet b-weight ($\mathcal{P}_b\left(w|p_{\mathrm{T}}\right)$) in bins of p_{T}, the flavour fractions f_{f_1,f_2}, the $\mathcal{P}_{f_1 f_2}\left(p_{\mathrm{T},1}, p_{\mathrm{T},2}\right)$ and the non-b-jet b-weight PDFs are determined from simulation.

A slightly more complex likelihood function is defined for the three-jet case, which is conceptually analogous but needs to consider that the jet flavour combinations are increased to four. Accordingly, there are up to $n! = 3! = 6$ equivalent jet combinations the likelihood needs to be summed over, as they are a priori indistinguishable in data. The formalism in this case is:

$$\begin{aligned}
\mathcal{L}\left(p_{\mathrm{T},1}, p_{\mathrm{T},2}, p_{\mathrm{T},3}, w_1, w_2, w_3\right) = \quad & [\quad f_{bbb}\mathcal{P}_{bbb}\left(p_{\mathrm{T},1}, p_{\mathrm{T},2}, p_{\mathrm{T},3}\right)\mathcal{P}_b\left(w_1|p_{\mathrm{T},1}\right)\mathcal{P}_b\left(w_2|p_{\mathrm{T},2}\right)\mathcal{P}_b\left(w_3|p_{\mathrm{T},3}\right) \\
& + \quad f_{bbj}\mathcal{P}_{bbj}\left(p_{\mathrm{T},1}, p_{\mathrm{T},2}, p_{\mathrm{T},3}\right)\mathcal{P}_b\left(w_1|p_{\mathrm{T},1}\right)\mathcal{P}_b\left(w_2|p_{\mathrm{T},2}\right)\mathcal{P}_j\left(w_3|p_{\mathrm{T},3}\right) \\
& + \quad f_{bjj}\mathcal{P}_{bjj}\left(p_{\mathrm{T},1}, p_{\mathrm{T},2}, p_{\mathrm{T},3}\right)\mathcal{P}_b\left(w_1|p_{\mathrm{T},1}\right)\mathcal{P}_j\left(w_2|p_{\mathrm{T},2}\right)\mathcal{P}_j\left(w_3|p_{\mathrm{T},3}\right) \\
& + \quad f_{jjj}\mathcal{P}_{jjj}\left(p_{\mathrm{T},1}, p_{\mathrm{T},2}, p_{\mathrm{T},3}\right)\mathcal{P}_j\left(w_1|p_{\mathrm{T},1}\right)\mathcal{P}_j\left(w_2|p_{\mathrm{T},2}\right)\mathcal{P}_j\left(w_3|p_{\mathrm{T},3}\right) \\
& + \quad (1,3,2) + (2,1,3) + (2,3,1) + (3,1,2) + (3,2,1)]/6,
\end{aligned} \tag{5}$$

where the various PDFs are defined in a similar way to the two jet case, and the last line reflects the sum of the likelihood function over all possible permutations of three jets.

In order to simplify the determination of $\mathcal{P}_{f_1 f_2 f_3}\left(p_{\mathrm{T},1}, p_{\mathrm{T},2}, p_{\mathrm{T},3}\right)$ from simulations, which otherwise requires prohibitive simulation statistics, the following factorisation assumption is made:

$$\mathcal{P}_{f_1 f_2 f_3}\left(p_{\mathrm{T},1}, p_{\mathrm{T},2}, p_{\mathrm{T},3}\right) = \mathcal{P}_{f_1}\left(p_{\mathrm{T},1}\right)\mathcal{P}_{f_2}\left(p_{\mathrm{T},2}\right)\mathcal{P}_{f_3}\left(p_{\mathrm{T},3}\right) \tag{6}$$

The effect of this approximation was tested, along with the entire fitting method, using MC closure tests. In these tests the fit procedure is applied to the Monte Carlo itself in order to check for possible biases. The tests have been performed for all four channels ($e\mu$ and $e^+e^- + \mu^+\mu^-$, 2 and 3 jets) and for several different b-tagging efficiency points. These tests all yield extracted efficiencies compatible with their known inputs within the statistical uncertainties, with systematic effects from non-closure found to be much less than 1%.

4 Systematic uncertainties

Systematic uncertainties are evaluated one by one, by replacing the Monte Carlo nominal sample with a sample affected by a single systematic uncertainty variation and then repeating the whole procedure. The result of the fit on the data then reflects this single systematic uncertainty. The variations observed on the b-jet efficiencies from all systematic uncertainties are then summed in quadrature to obtain the final systematic uncertainty on the result.

The main systematic uncertainties affecting the flavour compositions as well as the PDFs for the kinematic distributions are related to the modelling of the top and background processes. These uncertainties are estimated by considering the following variations:

- Hadronisation ($t\bar{t}$): Powheg+Pythia is compared to Powheg+Herwig to estimate the impact of the modelling of the showering and hadronisation of quarks/gluons in the simulated $t\bar{t}$ events, with the

full difference in the result assigned as a systematic uncertainty. This also probes the sensitivity to different models of b-hadron fractions, decays, and lifetimes.

- Modelling ($t\bar{t}$): POWHEG+HERWIG is compared to ALPGEN+HERWIG to compare NLO and multi-leg calculations for $t\bar{t}$. This also probes the difference between $t\bar{t}$ + $b\bar{b}$ where the $b\bar{b}$ is from parton shower only (POWHEG) or also from the matrix element (ALPGEN). Again the full difference is considered as a systematic uncertainty.

- Top p_{T} reweighting ($t\bar{t}$): The uncertainty on the top p_{T} reweighting is taken as 100% of the correction (Section 2.3).

- More/less PS ($t\bar{t}$): Comparison of the ACERMC $t\bar{t}$ MC tuned to include more and less parton shower radiation. As these samples represent two extreme scenarios, half the difference is taken as an uncertainty on initial and final state radiation from the parton shower.

- More/less PS (single top): Comparison of the ACERMC single top Wt-channel MC with more and less parton shower radiation, again taking half of the difference to estimate the uncertainty on initial and final state radiation from the parton shower.

- Modelling (Z+jets): SHERPA is compared to ALPGEN to estimate an uncertainty on the modelling of the Z+jets background.

- Modelling (dibosons): ALPGEN is compared to HERWIG, with half the difference taken as the uncertainty. This corresponds to an inclusive $\sim$ 50 % normalisation uncertainty on diboson production in the two-jet bin and $\sim$ 66 % in the three-jet bin.

Normalisation uncertainties are considered for the following processes:

- Normalisation single top: The relative top to single top normalisation is varied by $\pm$25 % in the two-jet bin and $\pm$35 % in the three-jet bin, motivated by scale uncertainties and parton density function systematic variations.

- Normalisation Z+jets: The normalisation is varied by $\pm$20 %, to account for the extrapolation uncertainty from the region where the scale factors are determined to the region where they are applied. The size of this variation is determined by comparing the data to Monte Carlo agreement in the relevant kinematic distributions.

- Normalisation Z+heavy flavour: The Z+heavy flavour component is varied by $^{+100}_{-50}$ % which is conservative compared to data/Monte Carlo variations observed in Z+b measurements [33].

- Normalisation lepton fakes: The fake lepton contribution is varied by $\pm$50 % as detemined from studies in data control regions.

In addition all relevant detector related systematic uncertainties are considered:

- Pile-up reweighting: The Monte Carlo is reweighted to describe the expected average number of interactions (μ) measured in data after scaling μ in the Monte Carlo simulation. The systematic uncertainty is estimated by varying the scaling factor by $\pm$3 %.

- Electron and muon efficiency, resolution and scale uncertainties: Lepton efficiencies, resolution and scale uncertainties are evaluated in analyses using large samples of candidate Z bosons decays.

- $E_{\mathrm{T}}^{\mathrm{miss}}$ soft-terms: The uncertainty due to the modelling of the soft-terms used in the $E_{\mathrm{T}}^{\mathrm{miss}}$ calculation. In addition the variation in the $E_{\mathrm{T}}^{\mathrm{miss}}$ due to the jet, electron and muon uncertainties are taken into account when the corresponding systematics are varied.

- Jet energy scale: The uncertainties are evaluated using analyses of dijet, γ+jet, and Z+jet samples, and their independent components, as discussed in Ref. [30], are applied separately.
- Jet energy resolution: This uncertainty is estimated by smearing the jets in simulated events according to the uncertainty on the resolution measured in the data [34].
- Jet vertex fraction: The uncertainty on the jet vertex fraction is estimated by varying the cut value for simulated jets to cover the observed discrepancies with the data.
- Mis-tag rate: The non-b-jet tagging rate in the simulation is corrected by the light-jet data to Monte Carlo scale factors measured in a dedicated calibration following Ref. [7], with the systematic estimated by varying the associated uncertainty. Due to the small c-jet contribution, they are combined with the light-flavour jets when evaluating this uncertainty.

In the combination of the different channels (two and three jets, $e\mu$ and $e^+e^-/\mu^+\mu^-$) all single systematic variations are treated as fully correlated, except for the theory uncertainties, for which a 50 % correlation is assumed. This is motivated by the fact that such uncertainties rely on an estimate provided purely by the difference between the two Monte Carlo generators and that the selections vary significantly among the different channels. In addition, it was checked that this assumption results only in minor differences in the final MC to data scale factors.

5 Results

The result of the combination of the four channels ($e\mu$ and $e^+e^-/\mu^+\mu^-$ channels in the two- and three-jet bins) is shown in Table 3 and graphically in Fig. 2 for the calibration in ten jet p_{T} bins in the region of 20 GeV $< p_{\mathrm{T}} <$ 300 GeV. A more detailed break-down of the systematics in bins of p_{T} is shown in Table 4. In general the data-to-simulation scale factors are consistent with unity within the statistical and systematic uncertainties of the measurements. The scale factors do not exhibit any significant trend as a function of jet p_{T} and are measured to a relative precision of ~ 2 % for jets in the p_{T} range 60–140 GeV.

p_{T} range (GeV)	Combined SF	Stat. error	Syst. error	Total error
20–30	0.968	0.022	0.059	0.063
30–40	0.979	0.012	0.030	0.033
40–50	0.986	0.010	0.027	0.028
50–60	0.985	0.010	0.023	0.025
60–75	0.971	0.009	0.020	0.022
75–90	0.980	0.010	0.015	0.018
90–110	0.965	0.010	0.018	0.020
110–140	1.000	0.010	0.020	0.022
140–200	0.989	0.014	0.033	0.036
200–300	1.008	0.032	0.077	0.084

Table 3: Scale factors obtained from combining the four different channels for the MV1 b-tagging tool at the 70 % b-jet efficiency working point. The statistical, systematic and combined uncertainties are shown separately for each jet p_{T} bin.

While previous calibration scale factors did not exhibit any significant η dependence, the increased precision offered by the present calibration analysis makes it interesting to verify this once more. To this end, the calibration analysis is repeated with the 30 GeV $< p_{\mathrm{T}} <$ 200 GeV range subdivided into four coarser p_{T} bins, each of which is subdivided into three jet $|\eta|$ regions: $0 < |\eta| < 0.7$, $0.7 < |\eta| < 1.5$ and $1.5 < |\eta| < 2.5$. The results in these different $|\eta|$ regions are shown in Fig. 3. Given the similarity of the

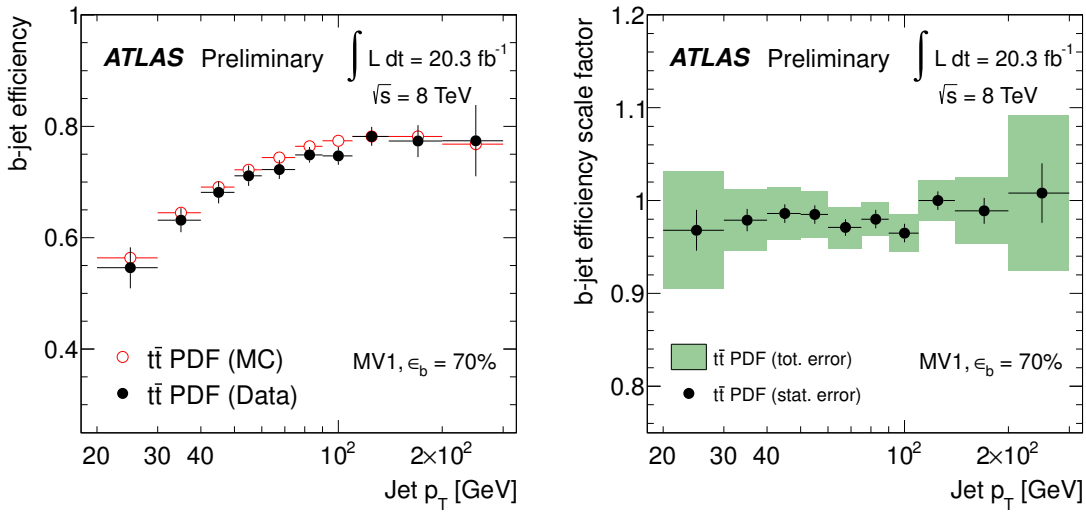

(a) *b*-jet efficiencies

(b) *b*-jet efficiency scale factors

Figure 2: The (a) *b*-jet efficiencies and (b) *b*-jet efficiency scale factors obtained from the combination of the four channels for the MV1 *b*-tagging tool at the 70 % *b*-jet efficiency working point. For (a) the error bars on the data points represent the total statistical and systematic uncertainties. For (b) both statistical only (black lines) and total errors (green shaded region) are shown.

p_T interval [GeV]	20-30	30-40	40-50	50-60	60-75	75-90	90-110	110-140	140-200	200-300
SF	0.968	0.979	0.986	0.985	0.971	0.980	0.965	1.000	0.989	1.008
Total error [%]	6.5	3.4	2.8	2.5	2.3	1.8	2.1	2.2	3.6	8.4
Stat. error [%]	2.3	1.2	1.0	1.0	0.9	1.0	1.0	1.0	1.4	3.2
Syst. error [%]	6.1	3.1	2.7	2.3	2.1	1.5	1.9	2.0	3.3	7.6
Systematic Uncertainties [%]										
Hadronisation ($t\bar{t}$)	1.0	0.6	1.5	1.4	1.1	0.5	0.8	0.3	1.0	2.0
Modelling ($t\bar{t}$)	1.1	0.4	1.0	1.1	1.0	0.5	0.7	0.9	0.7	1.7
Top p_T reweighting ($t\bar{t}$)	0.2	0.3	0.3	0.2	0.2	0.1	0.1	0.4	1.4	4.6
More/less PS ($t\bar{t}$)	0.5	0.6	0.9	0.8	0.9	1.0	0.9	0.8	1.4	1.9
More/less PS (single top)	0.2	0.0	0.1	0.1	0.2	0.1	0.2	0.2	0.0	0.0
Modelling (Z+jets)	0.8	0.3	0.2	0.5	0.3	0.2	0.3	0.3	0.9	2.4
Modelling (dibosons)	0.7	0.7	0.6	0.6	0.6	0.6	0.7	0.8	1.3	3.1
Norm. single top	0.5	0.4	0.3	0.2	0.2	0.2	0.2	0.2	0.3	0.0
Norm. Z+jet	0.9	0.6	0.9	0.4	0.7	0.5	0.6	0.7	1.1	1.7
Norm. Z+b/c	0.1	0.1	0.2	0.1	0.1	0.0	0.1	0.0	0.1	0.2
Norm. lepton fakes	0.3	0.3	0.2	0.3	0.2	0.2	0.3	0.3	0.3	0.4
Pile-up reweighting	0.1	0.1	0.1	0.1	0.1	0.0	0.0	0.0	0.0	0.1
Electron eff./res./scale	0.1	0.1	0.2	0.1	0.1	0.1	0.1	0.1	0.1	0.1
Muon eff./res./scale	0.2	0.3	0.2	0.3	0.1	0.2	0.1	0.1	0.0	0.0
$E_{\mathrm{T}}^{\mathrm{miss}}$ soft-terms	0.1	0.1	0.2	0.0	0.2	0.0	0.1	0.2	0.3	0.5
Jet energy scale	4.1	2.2	1.2	0.7	0.7	0.3	0.7	0.8	1.2	2.6
Jet energy resolution	2.6	1.0	0.3	0.3	0.1	0.2	0.2	0.0	0.2	0.2
Jet vertex fraction	0.8	0.1	0.0	0.1	0.1	0.1	0.2	0.2	0.2	0.2
Mis-tag rate	2.8	1.1	0.5	0.4	0.3	0.2	0.3	0.4	0.5	1.1

Table 4: Systematic uncertainties on the MC to data scale factors measured for the combined result using the MV1 *b*-tagging tool at the 70 % *b*-jet efficiency working point.

measurements in each $|\eta|$ bin as a function of jet p_{T}, the most stringent test is obtained by comparing the results as a function of $|\eta|$ inclusively in p_{T}. A χ^2 test is carried out to determine the compatibility of the result with a constant value. The systematic correlations are taken into account for the χ^2 compatibility test with no dependence on $|\eta|$ assumed. The probability to find a worse χ^2 value is 97%; in conclusion, no significant $|\eta|$ dependence is observed.

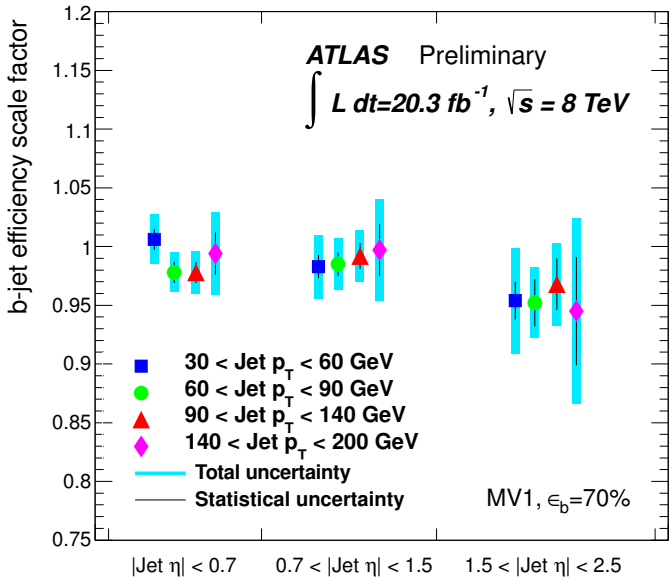

Figure 3: The η dependence of the scale factors in different p_{T} bins for the MV1 b-tagging tool at the 70 % b-jet efficiency working point. The p_{T} binned scale factors are calculated in three η regions: $0 < |\eta| < 0.7$, $0.7 < |\eta| < 1.5$ and $1.5 < |\eta| < 2.5$. The error bars on the points represent the total statistical and systematic uncertainties.

6 Conclusion

Results have been presented for a measurement of the b-jet tagging efficiency on a sample of $t\bar{t}$ events in the dilepton decay channel using a novel combinatorial likelihood approach with 20.3 fb^{-1} of data collected at $\sqrt{s} = 8$ TeV. The b-jet tagging efficiency measurements are provided in the form of jet transverse momentum dependent scale factors which correct the b-tagging performance in simulation to that observed in data. The scale factors have been measured in the jet p_{T} range 20–300 GeV, with good agreement observed between the data and simulated tagging efficiencies. A total uncertainty on the scale factors of ~ 2 % for jets with p_{T} around 100 GeV for the MV1 b-tagging tool at the 70 % b-jet efficiency working point is achieved, which represents a significant improvement in precision compared to alternative calibration methods.

References

[1] ATLAS Collaboration, *The ATLAS Experiment at the CERN Large Hadron Collider*, JINST **3** (2008) S08003.

[2] ATLAS Collaboration, *The ATLAS Simulation Infrastructure*, Eur. Phys. J. **C70** (2010) 823–874, arXiv:1005.4568 [physics.ins-det].

[3] ATLAS Collaboration, *Commissioning of high performance b-tagging algorithms with the ATLAS detector*, ATLAS-CONF-2011-102, https://cds.cern.ch/record/1369219.

[4] ATLAS Collaboration, *Measurement of the b-tag Efficiency in a Sample of Jets Containing Muons with 5 fb^{-1} of Data from the ATLAS Detector*, ATLAS-CONF-2012-043, https://cds.cern.ch/record/1435197.

[5] ATLAS Collaboration, *Measuring the b-tag efficiency in a $t\bar{t}$ sample with 4.7 fb^{-1} of data from the ATLAS detector*, ATLAS-CONF-2012-097, https://cds.cern.ch/record/1460443.

[6] ATLAS Collaboration, *b-jet tagging calibration on c-jets containing D^{*+} mesons*, ATLAS-CONF-2012-039, https://cds.cern.ch/record/1435193.

[7] ATLAS Collaboration, *Measurement of the Mistag Rate with 5 fb^{-1} of Data Collected by the ATLAS Detector*, ATLAS-CONF-2012-040, https://cds.cern.ch/record/1435194.

[8] P. Nason, *A new method for combining NLO QCD with shower Monte Carlo algorithms*, JHEP **11** (2004) 040, arXiv:0409146 [hep-ph].

[9] T. Sjöstrand, S. Mrenna, and P. Z. Skands, *PYTHIA 6.4 Physics and Manual*, JHEP **05** (2006) 026, arXiv:0603175 [hep-ph].

[10] P.Z. Skands, *Tuning Monte Carlo Generators: The Perugia Tunes*, Phys. Rev. **D82** (2010) 074018, arXiv:1005.3457 [hep-ph].

[11] H. L. Lai et al., *New parton distributions for collider physics*, Phys.Rev. **D 82** (2010), arXiv:1007.2241 [hep-ph].

[12] M. Mangano et al., *ALPGEN, a generator for hard multiparton processes in hadronic collisions*, JHEP **07** (2003) 001, arXiv:0206293 [hep-ph].

[13] C. Corcella et al., *HERWIG 6: An event generator for hadron emission reactions with interfering gluons (including supersymmetric processes)*, JHEP **101** (2011) 010, arXiv:0011.363 [hep-ph].

[14] J. F. J.M. Butterworth and M. Seymour, *Multiparton interactions ion photoproduction at HERA*, Z. Phys. (1996) 637, arXiv:9601.371 [hep-ph].

[15] J. Pumplin et al., *New generation of parton distributions with uncertainties from global QCD analysis*, JHEP **07** (2002) 012, arXiv:0201195 [hep-ph].

[16] B. P. Kersevan and E. Richter-Was, *The Monte Carlo event generator AcerMC version 2.0 with interfaces to PYTHIA 6.2 and HERWIG 6.5*, arXiv:hep-ph/0405247 [hep-ph].

[17] ATLAS Collaboration, *Measurement of $t\bar{t}$ production with a veto on additional central jet activity in pp collisions at $\sqrt{s}$ = 7 TeV using the ATLAS detector*, Eur. Phys. J. **C72** (2013) 2043, arXiv:1203.5015 [hep-ph].

[18] ATLAS Collaboration, *New ATLAS event generator tunes to 2010 data*, ATLAS-PHYS-PUB-2011-008, https://cds.cern.ch/record/1345343.

[19] ATLAS Collaboration, *ATLAS tunes of PYTHIA6 and Pythia8 for MC11*, ATLAS-PHYS-PUB-2011-009, https://cds.cern.ch/record/1363300.

[20] T. Gleisberg et al., *Event generation with SHERPA 1.1*, JHEP **02** (2009) 007, arXiv:0811.4622 [hep-ph].

[21] ATLAS Collaboration, *Measurement of the $t\bar{t}$ production cross-section in pp collisions at $\sqrt{s}$ = 8 TeV using eμ events with b-tagged jets*, ATLAS-CONF-2013-097, https://cds.cern.ch/record/1600596.

[22] ATLAS Collaboration, *Expected Performance of the ATLAS Experiment – Detector, Trigger and Physics*, CERN-OPEN-2008-020, https://cds.cern.ch/record/1125884.

[23] ATLAS Collaboration, *Performance of the ATLAS Secondary Vertex b-tagging Algorithm in 7 TeV Collision Data*, ATLAS-CONF-2010-042, https://cds.cern.ch/record/1277682.

[24] M. Cacciari, G. P. Salam, and G. Soyez, *The anti-k_t jet clustering algorithm*, JHEP **04** (2008) 063, arXiv:0802.1189 [hep-ph].

[25] M. Cacciari and G. P. Salam, *Dispelling the N^3 myth for the k_t jet-finder*, Phys. Lett. **B641** (2006) 057, arXiv:0512210 [hep-ph].

[26] M. Cacciari, G. P. Salam, and G. Soyez. http://fastjet.fr/.

[27] M. Cacciari and G. P. Salam, *Pileup subtraction using jet areas*, Phys. Lett. **B659** (2008) 119–126, arXiv:0707.1378 [hep-ph].

[28] ATLAS Collaboration, *Pile-up subtraction and suppression for jets in ATLAS*, ATLAS-CONF-2013-083, https://cds.cern.ch/record/1570994.

[29] ATLAS Collaboration, *Jet energy measurement with the ATLAS detector in proton-proton collisions at $\sqrt{s}$ = 7 TeV*, Eur. Phys. J. **C73** (2013) 2304, arXiv:1112.6426 [hep-ex].

[30] ATLAS Collaboration, *Jet energy scale and its systematic uncertainty in proton-proton collisions at $\sqrt{s}$ = 7 TeV with ATLAS 2011 data*, ATLAS-CONF-2013-004, https://cds.cern.ch/record/1509552.

[31] ATLAS Collaboration, *Measurement of top quark pair differential cross-sections in the l+jets channel in pp collisions at $\sqrt{s}$ = 7 TeV using the ATLAS detector*, ATLAS-CONF-2013-099, https://cds.cern.ch/record/1600778.

[32] F. James and M. Roos, *Minuit: A System for Function Minimization and Analysis of the Parameter Errors and Correlations*, Comput. Phys. Commun. **10** (1975) 343–367.

[33] ATLAS Collaboration, *Measurement of the cross-section for b-jets produced in association with a Z boson at $\sqrt{s}$ = 7 TeV with the ATLAS detector*, Phys. Lett. **B706** (2012) 295–313, arXiv:1109.1403 [hep-ex].

[34] ATLAS Collaboration, *Jet energy resolution in proton-proton collisions at $\sqrt{s}$ = 7 TeV recorded in 2010 with the ATLAS detector*, Eur. Phys. J. **C73** (2013) 2306, arXiv:1210.6210 [hep-ex].